

Paxel: A Generic Framework to Superimpose High-Frequency Print Patterns using Projected Light

Petar Pjanic and Anselm Grundhöfer

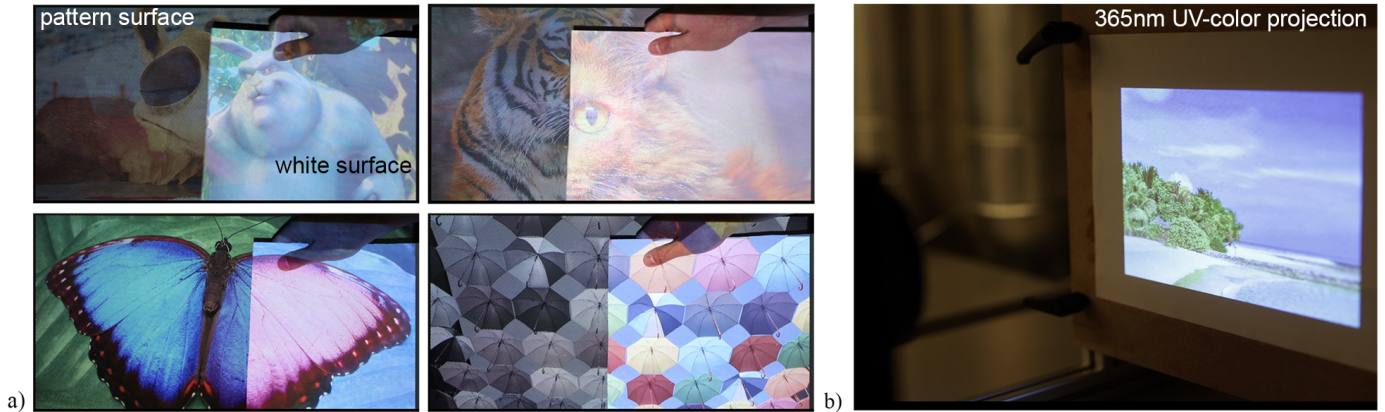


Fig. 1: Our framework enables a variety of applications: (a) Shows *color-changing effects* occurring when the projection surface is switched from a high-frequency *pattern* to a *white surface*. The effect is shown by holding a white paper in front of the *pattern*. In (b) a *monochrome-to-color* projection is achieved by projecting 365nm UV light onto a pattern consisting of invisible fluorescent red, green and blue pigments. All images are taken with automatic aperture and white balance.

Abstract—In this paper, we propose *Paxel*, a generic framework for modeling the interaction between a projector and a high-frequency *pattern surface*. Using this framework, we present two different application setups (cf. Fig. 1a): a novel *color-changing effect*, created with a single projected image and only when the projection surface is changed from a *pattern surface* to a *uniform white surface*. The observed effect relies on the spatially different reflectance properties of these two surfaces. Using this approach, one can alter color properties of the projected image such as hue or chroma. Furthermore, for a specific color range, defined by an *full color-changing sub-gamut*, one can embed two completely different images, within a single static projection, from which either one will be revealed depending on the surface. The second application allows the creation of color images using a single channel projector. For this application, we present a full color projection created using a 365 nm ultraviolet (UV) projector in combination with fluorescent pigments (cf. Fig. 1b), enabling new display possibilities, such as projection through participating media, e.g. fog, while hiding the scattering of the projection light outside of the visible spectrum. Both presented approaches create effects that might be striking to the observer, making this framework useful for art exhibitions, advertisements, entertainment and visual cryptography. Finally, in Sec. VI, we provide an in-depth analysis of the reproducible colors based on input parameters, used in the presented algorithm, such as: pattern layout, dot size of the pattern and the number of the clusters formed by k-means algorithm (IV-B).

Index Terms—projection, color-changing effect, color prediction model, pattern surface, 365nm UV-color projection, dual-image projection, hue-shifts, monochrome-to-color projections.

P. Pjanic and A. Grundhöfer are with Disney Research, Zurich, Switzerland. e-mail: (petar.pjanic@disneyresearch.com, anselm@disneyresearch.com).

This paper has supplementary downloadable material available at <http://ieeexplore.ieee.org>, provided by the author. The material includes video/Paxel.mp4. Contact anselm@disneyresearch.com for further questions about this work.

I. INTRODUCTION AND MOTIVATION

The quality of projectors has significantly improved in terms of resolution, dynamic range, frame rate, power consumption, and color gamut. They are used in a variety of applications, ranging from digital cinema, home entertainment, and interactive displays to projection mapping and dynamic art installations. Accurate manipulation of the projected light is still an ongoing field of research, especially with respect to widening the application potential of such devices. In the fabrication community, the creation of novel color reproduction techniques and the generation of striking *color-changing effects* (appendix A contains table of terms) is an active field of research. Regarding projection systems and color reproduction, a lot of exploration has been carried out to change the projection image to account for the illuminated surface pigments. Some of this research is focused on a per-pixel color compensation to generate correct color reproduction.

However, if the projection surface contains small color dots arranged in a repetitive, high-frequency layout, the human eye might not be able to distinguish between each of the individual dot colors. Instead, it averages this high-frequency color information into a single color.

Based on this observation, we propose *Paxel*, a framework that enables accurate color reproduction and the creation of *color-changing effects* by projecting spatially varying light onto high-frequency patterns. The framework is generic and can account for any number of illumination channels (*i.e. projector colors*), as well as different *colorants* (the colors present on the projection surface). Two sample applications will be presented as well:

A. Color-Changing Effect

We present a novel color-changing effect that occurs with a single, static projection and only when the projection surface is changed from a *pattern surface* to a uniform *white surface*. The observed image can significantly change its color properties such as hue, chroma, or even change to a completely different image (chroma refers to saturation of the color and hue to the type of the color such as yellow, blue, red etc.).

The main motivation for this approach is that the setup is static. One needs to register the projector to the *pattern surface*; however, the *white surface* can be freely moved since the color-changing effect is created due to the difference in reflectance properties between the two surfaces, i.e., this approach does not need to know the orientation of the second *white surface*.

B. Monochrome-to-Color Projections

The proposed framework also enables us to generate color images from a single channel projection using spatial reflectance multiplexing. For this application, the *pattern surface* consists of repetitive high-frequency *rgb* dots. By selectively illuminating a combination of these *colorants* (i.e. the *rgb* dots), a variety of colors can be generated. One beneficial application would be to print visible *rgb colorants* and illuminate them with a white light DLP (Digital Light Processing) projector. Compared to time-sequential DLP color projection, this approach reduces the spatial resolution of the projector, but has the advantage of tripling the frame rate while preserving a similar overall luminance.

A second application of this approach enables us to create emissive color displays using projected UV light. Therefore, the *pattern surface* is printed using invisible fluorescent *rgb* pigments. These inks are stimulated to emit visible light when illuminated with 365 nm light. In this paper we will show that it is possible to create full-color projections using a single-channel DLP UV projector (cf. Sec. V-B).

C. Our Contribution

In summary, we present the following original contributions:

- A generic framework modeling the interaction between *projected light* and a high-frequency *pattern surface*.
- A novel color-changing effect generated when the surface is switched from a *pattern surface* to a *white surface*.
- A UV projection setup enabling us to create color images by projecting 365 nm light onto *rgb* fluorescent inks.
- A precise projector pixel classification according to the *colorant* that it illuminates and a highly accurate color prediction model tested on different devices.
- An alternative image-based color prediction approach considering spatial variations such as projector lens aberrations such as vignetting and defocus .
- Relying on a halftoning, i.e., spatial-thresholding technique used in printing community [1, pp.385-491], we present image-assembly technique enabling us to project images in native projector resolution.
- An in-depth analysis of application-specific achievable color-gamuts, the influence of different *pattern* structures,

and the intensity of the generated colors depending on both printed dot size and the number of classified pixel *clusters*.

In the following, we refer to the projection surface that consists of high-frequency color dots as "*pattern surface*", to a projection surface that is uniformly white "*white surface*". Individual colors that are present in the *pattern surface* are referred to as "*colorants*", and the individual projected color channels will be named "*projector color*". Groups of projector pixels, that are deduced based on which printed *colorant* they illuminate, are referred as "*clusters*". The individual colors red, green, and blue will be abbreviated by "*r*", "*g*", and "*b*", and the term "black and white" will be shortened to "*b/w*". The rest of terms and abbreviation are shown in appendix A.

The remainder of this paper is organized as follows: We start by a related work discussion (Sec. II), and then explain the basic principles of the color formation (Sec. III). In Sec. IV, we show how to group projected pixels into *clusters* and how to predict the observed color in depending on the projection input. In Sec. V, we show the work-flows to create both *color-changing* and *monochrome-to-color* applications, as well as results. An in-depth pattern analysis and limitations are stated in Sec. VI, and in Sec. VII, we finally give a summary and an outlook of potential future improvements.

II. BACKGROUND AND RELATED WORK

The method we are presenting crosses several active research fields, mainly color-changing effects with techniques such as customized printing patterns, color appearance models, and the geometric and photometric calibration of projector-camera systems (*procams*). The most relevant related publications and how they differ from the presented work will be discussed in the following section.

A. Projection onto Non-White Surfaces

Projecting images onto non-white and textured surfaces while neutralizing or otherwise manipulating the surface appearance has been widely investigated under the terms radiometric [2]–[4] [5], [6] or photometric compensation [7], [8], where a *procams* is used to analyze the reflectance of a diffuse surface and to alter the intensity and color of each individual pixel such that the desired image is perceived when the processed image is projected onto the surface. In [9], this idea was extended to also compensate for global light transport effects when projecting onto a non-perfectly diffuse surface. Similar extensions for compensating effects of local light transport have also been proposed by others [10]–[12], while in [13], the method was extended to adapt to a dynamically changing surface texture. A method of increasing the dynamic range of a static planar projection surface has been presented by Bimber and Iwai [14] and further extended for complex textured geometries by [15]. In [16], Jones and colleagues present a computationally optimized projection surface that enables a contrast enhancement targeted onto a specifically known input animation. Similarly, Amano [17] as well as Kawabe [18] presented methods to change the perception of a

static print into hue- and luminance-adapted animated images by the use of a coded projection and registered print setup.

Although the latter approaches also proposed the generation of a distinct surface to increase the image quality, we suggest an adapted projection onto a generic pattern that is independent of the content and thus enables a variety of effects for arbitrary input data.

Sun et al. [19] enhanced the contrast of projected images by using a black projection screen composed of stacked layers of emissive r , g and b fluorescent dyes which are excited when illuminated with specific visible and near-UV wavelengths. In contrast to this method, we are presenting a method using a single (365nm), invisible monochrome illumination to excite invisible r , g and b fluorescent pigments printed side by side in a high frequency spatial arrangement. Furthermore, our approach allows us to achieve additional effects such as projecting through participating media without generating a visible trail (Fig 14) since no visible illumination is required at all.

B. Color-Appearance Models

Color-appearance models are used to describe how the human eye perceives a given color stimulus. These models account for various effects, e.g. chromatic and luminance adaptation (i.e. how the eye adjusts its processing depending on the situation) and are separated into two main groups: *global* and *local* color-appearance models.

The *global* color-appearance models assume that the human eye adapts equally to the overall observed scene, disregarding any spatially local adaptation. One of the most used *global* color-appearance model is CIELAB [20, pp. 201-210] which is simple to master, widespread and considered to be the *de facto* international standard in colorimetry. In contrast, more advanced color-appearance models, such as CIECAM02 [20, pp. 287-301], are able to much more accurately account for more complex visual effects but have significantly higher computational complexity and a large number of input parameters.

Local color-appearance models rely on the fact that the adaptation state of the eye depends on the spatial content that is being observed. Wallach [21] introduced the luminance ratio model showing that the luminance of an observed stimulus depends on the luminance of the surrounding stimulus. Based on this luminance ratio model, Land and McCann [22] introduced the Retinex theory showing that strong edges in the observed scene have a crucial impact on the state of eye adaptation. Rudd and Zermach [23] further extended the Retinex theory and luminance ratio model by introducing the weighed log luminance ratio model (WLLR). Gronchi and Provenzi [24] proposed a general framework to describe such context-related effects that are suitable for physical as well as non-physical judgments. Vangorp et. al. [25] presented a model of local adaptation by performing comprehensive sets of visual experiments and selecting the best local adaptation model according to these experiments.

In our experiments, the projection surface is uniformly illuminated and the *pattern surface* consists of high frequency patterns avoiding strong perceivable edges. Because of this,

in our setup, we do not consider any local adaptation effects, allowing us to successfully use *global* color-appearance model (CIELAB) to model the observed colors.

C. Color-Alteration Effects and Revealing Hidden Content

Revealing hidden or presenting multiple different images using specialized hardware is a wide and active field of research. In [26], a 3D surface structure was optimized such that different images were generated out of the cast shadows depending on the illumination direction. Pappas et al. developed a method to reveal images hidden steganographically using refractive elements, such as custom-built lenses [27]. Hersch et al. developed a variety of methods to embed hidden imagery within prints using specialized ink components, such as metallic [28] or fluorescent ones [29], and moiré generating printing patterns [30]. In [31], [32], methods were presented to encode two images with varying luminance, hue, and completely different appearances using specific prints on a metallic substrate. Baar et.al. proposed an algorithm to reduce ghosting artifacts in lenticular relief prints [33]. Another related research field focuses on visual cryptography where image are encoded using random operators within multiple printed transparent sheets such that the image content is only revealed when carefully superimposed but is otherwise imperceivable [34]–[36]. In a similar research field, Chosson and Hersch created beating shapes relying on moiré level lines [37].

Displays and projectors were also used to embed varying images that can be revealed either by active temporal shuttering [38], varying wavelengths [39], or polarizing filters [40]. These methods are mostly used for a per-eye image separation needed for stereoscopic displays. The encoding can also be adjusted depending on the observation position, for example, for auto-stereoscopic displays using lenses, parallax barriers or for light field displays [41], [42].

D. Summary

Our method, although having overlaps with the presented research contributions, targets a different goal: it is focused on the combination of a projection with registered high-frequency printed patterns to enable various interesting effects, ranging from gray-scale projections being transformed into reflected full-color images, image hiding, and watermarking, to arbitrary *dual-image projections*. The *dual-image projections* is an effect where two completely different images are revealed one on the *pattern surface* and another on the uniform *white surface*. This approach can also be used to transform invisible UV light into full-color *rgb* images using fluorescent micro-patches. How these effects can be achieved will be described in the following sections.

III. COLOR EFFECTS AND COLOR FORMATION

Before going into more detail, we describe the core principles on how the workflow generates a specific color effect by using three examples. The first two will describe how to generate *color-changing effects* by using a *pattern surface* containing *b/w* pigments or consisting of various

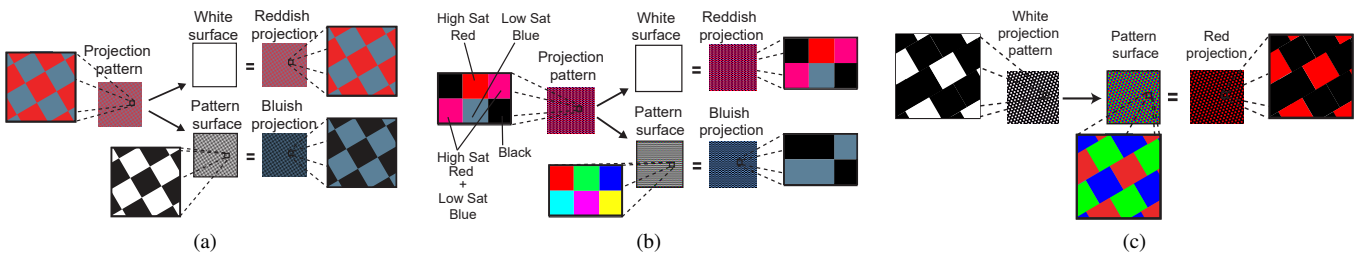


Fig. 2: (a) Projecting a highly saturated red and a low saturated blue color onto a *white surface* results in a reddish surface appearance. When the same pattern is projected onto a *pattern surface*, where the red color is absorbed by the printed black ink, an overall bluish appearance is perceived. For illustration purposes the printed black dots and red projection are in exact superpositions. (b): Projecting a highly saturated red color onto all *colorants* that absorb red wavelengths and a low saturated blue color onto all *colorants* that reflect the blue wavelengths. When projected onto the *pattern*, the red is absorbed, resulting in a bluish appearance. The same projection observed on a *white surface* generates a reddish appearance, since red is no longer absorbed. (c) Monochrome-to-color projection. Illuminating different parts of the *pattern surface* enables us to generate different colors.

color pigments. The third example shows how to generate *monochrome-to-color* projections. Both the *color-changing* effect and *monochrome-to-color* projection can be achieved with various high-frequency pattern layouts, such as checkerboard arrangements or blue-noise random distributions. However, the specific layout can have a significant impact on the intensity of the generated color, pattern visibility, and the formation of disturbing aliasing artifacts, such as moiré [43] (cf. Sec. VI). For simplicity, in the following examples, the *pattern surface* is composed of a repeatable tile structure (Figs. 2a-2c)

A. Color-Changing Effect with a B/W Pattern Surface

The generation of color alterations relies on the *color-changing* effect created with a single projected image and only when the projection surface is switched from the *pattern surface* to a uniform *white surface*. In this first example, we are projecting *rgb* color intensities using a video projector onto a high-frequency *b/w* pattern. We want to intuitively show how to create the simple *color-changing* effect: a blue color should be observed when projecting onto the *pattern surface*, and a red color when the same content is projected onto a uniform *white surface*.

If a highly saturated red color is projected only onto regions where black pigments are printed and a low saturated blue color on all the remaining ones, i.e., the white areas, the majority of the projected red color will be absorbed by the black pigment. This results in an overall blueish surface appearance. However, when the same image intensities are projected onto a uniform *white surface*, the red projection is no longer absorbed by the black pigment. Now, since the red projection has a higher saturation compared to the blue projection, an overall reddish surface appearance is perceived, i.e., when the strong red and weak blue colors are projected in a high-frequency arrangement, the human eye averages these projected colors in the local neighborhood, and a reddish color tone is observed. Fig. 2a shows the illustration of this red-to-blue color change.

B. Color-Changing Effect with a Colored Pattern Surface

Instead of a high-frequency *b/w* pattern, the same principle can also be used to create a *color-changing* effect by projecting onto colored *pattern surfaces*. In this example, the high-frequency pattern is composed of small cyan, magenta, yellow,

red, green, and blue printed pigments (cf. Fig. 2b). It illustrates the same *color-changing* effect, as shown in Sec. III-A, now achieved when projecting onto a colored *pattern surface*: A highly saturated red color is projected onto all printed *colorants* that absorb the red color, e.g., *g*, *b*, and *c* pigments, and a low saturated blue color is projected onto all printed *colorants* that reflect the blue color, e.g., *m*, *b*, and *c*. Similar to Sec. III-A, the vast majority of the projected red color is absorbed on the *pattern surface*, resulting in a blueish appearance. In contrast, when projecting the same pattern onto a uniform *white surface*, the high saturated red is no longer absorbed, leading to a reddish appearance.

C. Monochrome-to-Color Projections

Besides the color changes, the same principle can be used to create full-color images by projecting a single-channel illumination, such as white light, onto a high-frequency *pattern surface* containing *rgb* pigments. Fig. 2c shows that by separately illuminating the *rgb* pigments, arbitrary color mixtures can be achieved. Similar to the color alterations, the pattern pigments are printed side by side at a high spatial frequency. As a result, the eye will average the *rgb* intensities to form a single color, similar in principle to using a Cathode Ray Tube (CRT) screen. Furthermore, as discussed in the introduction, this approach enables us to generate color images using a monochrome 365 nm UV-projector illuminating fluorescent *rgb* pigments.

IV. METHOD

To achieve the proposed effects, we present Poxel a generic framework consisting of the following steps required for all potential applications:

- 1) **Geometric Calibration:** Accurately registering the projector pixels to the *pattern surface* using a camera.
- 2) **Clustering:** Classifying each projector pixel according to the *colorant* pigment it illuminates.
- 3) **Color Prediction:** Establishing a model enabling an accurate estimate of the reflected color.

Each step will be discussed in detail in the remainder of this Section.

A. Geometric Calibration

To establish correspondences between each projector pixel and the *colorants* on the *pattern surface*, we perform a 2D geometric registration and mapping using a projector-camera system (*procams*), i.e., we establish a highly precise geometrical mapping of corresponding projector and camera pixels enabling the warping of the desired target images to the projector’s perspective and in projectors resolution.

The first step is to manually align the projection as accurately as possible with respect to the surface in terms of its optical axis and focus. Then, a camera is set up such that it is observing the printed pattern surface perpendicular to its optical axis with a stopped down aperture to ensure that the surface is well focused. Having this carried out, structured light patterns are projected to generate a geometric relationship between each individual projector and camera pixel. Therefore, a sub-pixel accurate method consisting of binary, complementary Gray Code patterns [44] in combination with thin, shifted lines [45] are projected, captured, and processed to generate a dense mapping between corresponding pixels.¹ The mapping is stored as a per-projector-pixel lookup table that can warp captured camera images onto the projector’s image plane. Individual pixels that were not reconstructed by the structured light process are interpolated from the detected nearest neighbors using Delaunay triangulation [46] and bilinear interpolation. The warped image, also called *nodal image*, is computed in the native projector resolution.

Depending on the quality of the used optical elements for the lenses, artifacts, such as chromatic aberrations might occur due to the varying wavelengths of the projected *rgb* colors. In order to account for such artifacts we separately generate the projection-camera mapping for each of the primaries, i.e., the structured light process is carried out individually for each projector channel, and individual lookup-tables, one for each channel, are generated.

B. K-means Clustering

After geometric calibration, the projector pixels are classified according to the *colorant* they illuminate, i.e., because of the nature of the color-formation (Sec. III) we need to determine/classify which projector pixel illuminates which printed *colorant*. To achieve this, the pattern surface is illuminated with a uniform, white projection, and the result is captured by the camera. This image is warped to the projector’s point of view using the individual per-color-channel lookup tables (cf. Sec.IV-A). These *nodal images* then represent, for each projector color-channel, which pixel illuminates which *colorant* on the *pattern surface* (cf. Fig.3a). Obviously, it is impossible to perfectly align all projector pixels to the printed pigments, and many pixels will hit an edge and thus illuminate several different *colorants*. This implies that the *nodal images* represent averaged values of the *colorants* each pixel illuminates. To avoid possible issues (wrong classifications) that could be caused by vignetting (spatial darkening of the projection caused by lens imperfections), we normalize all

nodal images with a nodal image of a white image illuminating a uniform *white surface*.

In the next step, all projector pixels of the *nodal images* are grouped/classified depending on the *colorants* they illuminate. Therefore, an approach inspired by [47] was applied: on each *nodal image* the K-means algorithm [48] is applied in CIELAB color space. Grouping pixels to a discrete number of primary colors significantly reduces the number of colors to classify. Fig.3b shows the result of a K-means operation using a *b/w* pattern and two clusters ($K = 2$). Here all projector pixels are classified into two groups depending on whether they mainly illuminate the black or the white surface areas. However if we specify $K = 3$, it will classify pixels into: mainly illuminating *b* or *w* areas, and an additional category that classifies all projector pixels that partly illuminate *b* and *w* pigments, which inevitably occurs at the border between the colorants (cf. Fig.3c).

The minimal number for K is equal to the number of colorants, e.g., for *b/w* print patterns $K_{min} = 2$, for *rgb* $K_{min} = 3$. Specifying K as a higher number gives more information and control over the projection, because it separates pixels that illuminate several *colorants*. However, raising the number of K also increases the complexity of the optimization function required to estimate the projection intensities (cf. Sec. V-A2 and V-B2) which makes it more difficult to converge. Furthermore, noise may be introduced, because the same color may be achieved with multiple solutions Please refer to Sec. VI-C for an in-depth discussion.

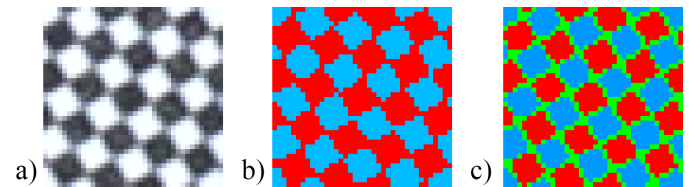


Fig. 3: K-means clustering applied to group pixels according to the *colorant* they illuminate: a) Shows the uniformly illuminated *b/w* print pattern. b) Color-coded result of the clustering using $K = 2$, separating pixels into mostly illuminating black (r) or white (b) areas. c) Using $K = 3$ separates pixels into mostly illuminating black (r), white (b), or both (g) areas.

C. Color-Prediction Model

Relying on the *clusters* deduced using the k-means algorithm, a color-prediction model can be constructed, enabling us to precisely predict the reflected color depending on the projected intensities, i.e., the reflected color is predicted as a modulation of projected light illuminating the *clusters*. In our setup, the number of illumination (i.e. projector color) channels does not has to be fixed to three *rgb* colors, but could also contain a monochrome light or any other number of channels. We present two approaches for predicting the reflected color: a *spectral approach* using measurements captured by a spectrophotometer and an *image-based approach* using the camera to acquire the required data.

1) *Spectral Approach*: As shown in Sec. IV-B, pixels are classified according to the *colorant* they illuminate. Because the *clusters* are small and arranged in a high-frequency pattern,

¹The interested reader is referred to [45] for a detailed evaluation of this method.

the contribution from each of the *clusters* to the overall observed color is additive:

$$R(\lambda) = \sum_{i=1}^K R_i(\lambda) \quad (1)$$

where $R(\lambda)$ is the overall reflectance of the surface illuminated by the projector, $R_i(\lambda)$ is the reflectance contribution of the i -th *cluster* and K is the number of clusters.

The color reflected from the each of the *clusters* $R_i(\lambda)$ is formed by illuminating *cluster* (i) with the *projector*. To model $R_i(\lambda)$, the potentially non-linear response functions of the projector channels have to be accurately measured and taken into account. Various algorithms exist to model the function ranging from simple gamma curves [49] to poly-harmonic spline mappings considering internal color processing, e.g., color mapping and black level boosting [8]. In our implementation we were able to disable any complex processing leading to input-dependent color-mixing allowing us to use a rather simple model as described in [50]. However more complex models accounting for such internal color processing can be used as well. The j response curve functions f_j , for each projector color channel, are obtained by measuring the projected colors for a dense set of intensities. Then, the responses are approximated by an interpolation function [51]. The shape of these curves strongly depends on the projector used.

To establish a model for $R_i(\lambda)$, we project the projector colors at full intensity only on the areas of the i -th *cluster* and measure the spectral response with the spectrophotometer $R_{j,i}^{f_i}$. Assuming that no projector-internal color processing occurs, we can calculate $R_i(\lambda)$ as a weighted sum of the projected colors at full intensity, projected only onto the i -th *cluster*. The weights $f_j(P_{j,i})$ are obtained by applying the response function onto the input intensity values:

$$R_i(\lambda) = \sum_{j=1}^N f_j(P_{j,i}) \cdot R_{j,i}^{f_i}(\lambda) \quad (2)$$

where $R_i(\lambda)$ is the reflectance of the i -th *cluster* illuminated with the projector, $R_{j,i}^{f_i}(\lambda)$ is the reflectance of the j -th projector color at full intensity projected only onto the i -th *cluster*, f_j is the response function for the j -th projector color channel, $P_{j,i}$ are input intensities for the j -th projector color channel projected only onto the i -th *cluster*, and N is the number of projector color channels.

It is important to mention that the spectrophotometer needs to be set up to capture the reflectance of a specific surface area covering multiples of all *clusters*, hence capturing the light that is spilled from one *cluster* to the another. This information is crucial to build an accurate spectral-prediction model.

Finally, we combine Eq. (2) with Eq. (1):

$$R(\lambda) = \sum_{i=1}^K \sum_{j=1}^N f_j(P_{j,i}) \cdot R_{j,i}^{f_i}(\lambda) \quad (3)$$

enabling us to predict the observed color as a function of input intensities $P_{j,i}$, i.e., how much of the j -th projector color is illuminating the i -th *cluster*. The final observed color is calculated as a weighted sum of all of the projection colors illuminating all *clusters*.

The benefit of this approach is that the same equations are used to predict the reflected color when the projection surface is changed from the *pattern surface* to the *white surface*. Therefore, only the reflectance $R_{j,i}^{f_i}$ has to be re-measured for the same patterns projected onto a uniform *white surface*.

Finally, we convert the predicted spectral reflectance to CIELAB device-independent color-space. The CIELAB colors are calculated by first converting the predicted spectra to the CIE-XYZ color space for the CIE 1931 Standard Observer, [52, pp. 156-157]. Then, the CIE-XYZ coordinates are converted to the CIELAB space by selecting the full-white projection illuminating the *white surface* as a white reference point [52, pp. 166-168]. We select this full-white projection as a white reference point, because it is the strongest stimulus that can be observed in the proposed setup.

2) *Image-Based Approach*: Although the color-prediction model based on spectral measurements creates colorimetrically accurate and convincing results, it has some drawbacks: Firstly, it requires a spectrophotometer, which is an expensive device and not widely available. Secondly, the modeling is based on a single, or several, spatial measurements that capture only a limited area of the projection.

To overcome these limitations, we propose a second approach based on using the camera to gather per-pixel information that then can be used to predict the reflected color for each individual projector pixel (x, y) . This enables us to account for spatial artifacts resulting from lens vignetting, light falloff, and spatially varying defocus. The necessary steps for an *image-based* color prediction approach are as follows:

- Capture camera images of all illumination channels projected onto all *clusters* at full intensity.
- Calculate the corresponding nodal images $R_{j,i}^{f_i}(x, y)$. They define the reflected r, g, b values for each projector pixel (x, y) , for each color at full intensity j and for each *cluster* i .
- The method assumes that the contribution of neighboring high-frequency clusters is additive. However, this is true only in a small spatial area. To model this property, we apply a Gaussian blur to the nodal images $R_{j,i}^{f_i}(x, y)$. The size of the kernel should be large enough to spread the information between *clusters*, but it strongly depends on the projector's resolution and the *pattern* dot size.
- A standard sRGB to CIE-XYZ conversion for D65 illumination is applied to convert the blurred nodal images to CIE-XYZ color space. Other conversions, such as for AdobeRGB or a device-dependent calibration can be used as well.
- Finally, similar to Eq. (3) a color-prediction function is defined to predict per-pixel CIE-XYZ color values in function of the input intensities:

$$R(x, y) = \sum_{i=1}^K \sum_{j=1}^N f_j(P_{j,i}) \cdot R_{j,i}^{f_i}(x, y) \quad (4)$$

where $R(x, y)$ is the predicted CIE-XYZ color for the projector pixel (x, y) , and $R_{j,i}^{f_i}(x, y)$ is the CIE-XYZ color of the j -th projector color at full intensity illuminating only the i -th *cluster* at pixel position (x, y) .

Compared to the *spectral approach*, the *image-based approach* requires less expensive hardware and accounts for spatial artifacts, such as vignetting, light falloff, and spatial defocus. However, the main drawback of the latter is the limited color precision during acquisition and conversion. In this regard, the *spectral approach* is more accurate. See appendix B for results generated with the *image-based approach*.

V. SAMPLE APPLICATIONS

In the following, we present two different applications of our proposed *Paxel* framework: a novel *color-changing effect* enabling us to change color-properties of the projected image, and a *monochrome-to-color projection* using a 365nm UV-projector.

A. Color-Changing Workflow

As schematically introduced in Section III, the *color-changing effect* is generated when the projection surface is switched from a *pattern surface* to a uniform *white surface*. The necessary steps to generate the *color-changing images* are as follows: testing the color-prediction model to ensure correct *color-changing effect* predictions, calculating color gamut volumes that describe achievable colors that can be used for a desired *color-changing effect*, incorporating an optimization function that estimates the optimal projection intensities that, when projected, create the desired effect, and finally assembling the projection image based on the computed projection intensities.

1) *Color-Prediction Accuracy and Achievable Color Gamuts*: Table I shows the color-prediction accuracy achieved using the spectral approach. The model was evaluated on both *white* and *pattern surfaces*. Therefore we used the 30° rotated *b/w* checkerboard pattern and $K = 2$. To cover the 6D space of the projection input ($3 \times 2 = 6$, 3 illumination channels and 2 clusters), we tested the color-prediction model on 100 random test projections.

TABLE I: Prediction accuracy of the spectral prediction model predicting the color-changing effect

Color-changing effect (ΔE_{00}^*)	mean	95% quantile	max
Pattern surface	1.9	3	5.9
White surface	2.36	3.8	8.5

The accuracy is expressed in the ΔE_{00}^* error metric commonly used to quantify the difference between two colors [20, pp. 83]). The average error between the predicted and measured colors is around 2, which proves that we can accurately predict color changes, which is beneficial to minimize artifacts such as ghosting.

Depending on the desired color-changing effect, the achievable sub-gamut can be deduced which will contain all the colors that enable the generation of the desired effect. In the following, we show estimated sub-gamuts that enable us to achieve a variety of color-changing effects (for the same setup used for the prediction accuracy evaluation), i.e., *b/w* pattern, 30° rotated checkerboard, $K = 2$. To estimate the shape and volume of the sub-gamuts, we use the method proposed by

Pjanic and Hersch [31]: The 6D input projection space $P_{j,i}$ is regularly sub-sampled in each dimension from min to max by 21 steps, resulting in $21^6 = 8576612$ input color values. For these sub-sampled input projections, we predict the resulting CIELAB colors on the *pattern* and uniform *white* surface. Let us deduce the sub-gamut that enables a specific color change, e.g., a hue-shift greater than 20°: Therefore, we sample the CIELAB color space with a step width of 1.0 and analyze for each sample color if there is a value that can reproduce this specific effect, e.g., if there is a $P_{j,i}$ that can achieve this hue-shift that is greater than 20°. All the colors that can achieve the desired color change form the shape and volume of the specific sub-gamut. Fig.4 shows the calculated sub-gamuts for various color-changing effects:

- The sub-gamuts that allow for specific hue shifts (Fig.4)a. The greater the hue shift, the more the available sub-gamut becomes less chromatic, but the lightness component stays intact compared to a full-projection gamut.
- The blue sub-gamuts shown in Fig.4b are computed for the generation of a decolorization effect. Any color that is located inside of this sub-gamut can change to its nearest achromatic color with a threshold of $\Delta E_{00}^* < 2$.
- The green line in Fig.4b depicts the sub-gamut allowing a neutralization of the image content, i.e., any color that lies inside can be changed into a single spatially consistent, uniform color. In this example we observe that the lightness component is reduced, resulting in projections that have less dynamic range compared to the full-projection gamut.
- The red area in Fig.4b shows the full color change sub-gamut that enables the creation of arbitrary dual-image projections. As expected, this full-color changing sub-gamut is quite small in volume, which results in relatively low-contrast and poorly saturated images. To estimate them, we specify two conditions: any color has to be able to change to its opposite color in hue domain and it has to be able to change to user-specified *b/w* colors (the optimal *b/w* can be approximated by an approach shown in Sec. VI-B).

It should be noted that the color-changing effects are asymmetric: Because the pattern surface reduces the overall amount of reflected light, the overall peak luminance is always lower compared to the projection on the white paper.

Similarly, sub-gamuts can be deduced for other pattern surfaces. However, sub-sampling of $P_{j,i}$ may become an issue for higher dimensional inputs because the dimensionality of $P_{j,i}$ directly depends on the number of printed colorants and K . A solution is to use a larger sub-sampling step width or an optimization technique to approximate the sub-gamut regions, as described in Sec. VI-B.

Once we have calculated the shape and volume of the sub-gamuts, we perform the gamut mapping of the input-image colors into the sub-gamut that produces the desired color-changing effect. The gamut mapping ensures the correct color-reproduction can be achieved. Once it has been performed, we use the optimization function, described in the following, to deduce the input projector intensities that we should project.

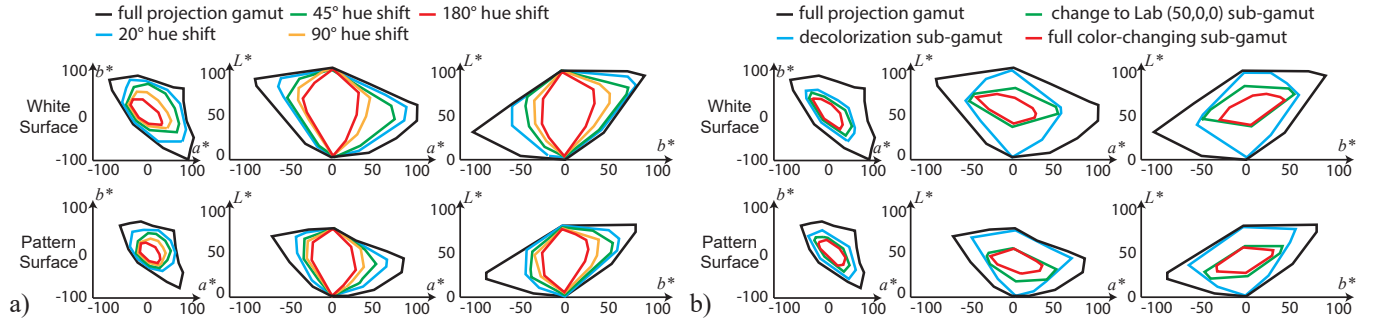


Fig. 4: Sub-gamuts for a desired hue-shift are shown in (a). In (b) other sub-gamuts are visualized: decolorization for a change to achromatic colors, a change to $Lab(50,0,0)$ defining the color volume to hide an image in a single CIELAB value, and for a full color-change where colors can be arbitrarily altered.

2) *Optimization Function*: Once we have deduced the available color range for a specific color-changing effect and performed gamut mapping, we can calculate the optimal input intensities which, when projected, produce the color-changing effect as close as possible to the target one. This is done by minimizing the square sum of two differences:

$$P_{j,i}^{Opt} = \arg \min((\Delta E_{00}^*(Lab_{T_{rgP}}, Lab_{\mathcal{P}}(P_{j,i})))^2 + (\Delta E_{00}^*(Lab_{T_{rgW}}, Lab_{\mathcal{W}}(P_{j,i})))^2) \quad (5)$$

where $Lab_{T_{rgP}}$ is the target CIELAB color that we want to observe on the *pattern*, $Lab_{T_{rgW}}$ the target CIELAB color that should be observed on a *white* surface, $P_{j,i}^{Opt}$ are the optimal intensities that, when projected, produce, as close as possible, the desired color changes. $Lab_{\mathcal{W}}(P_{j,i})$ is a CIELAB color observed on the white surface of the optimal projections $P_{j,i}$, and $Lab_{\mathcal{P}}(P_{j,i})$ is the CIELAB color observed on the pattern surface of the optimal projections. $Lab_{\mathcal{W}}(P_{j,i})$ and $Lab_{\mathcal{P}}(P_{j,i})$ are calculated by first estimating the reflectance using the color-prediction model and converting these values to CIELAB color space, as described in Sec.IV-C.

3) *Projection Image Generation*: The generation of the color-changing projections starts by specifying two different images that should be revealed when projecting onto the *pattern* or the *white* surface. These input images are transformed to the projector image plane, and their colors are converted from their input space (sRGB or AdobeRGB, etc.) to CIELAB color space and gamut mapped to the dedicated sub-gamut, enabling the desired color-change (cf. Sec.V-A1). Then, for each pixel coordinate, we use the gamut-mapped values as target colors in Eq. 5 and estimate $P_{j,i}^{Opt}$. These values describe how much of the j -th illumination channel should be projected onto the i -th *cluster*. This implies that each pixel illuminates all *clusters* in the same area. Because, however, each pixel only illuminates one specific *cluster*, further processing is needed.

A simple approach would be to merge $n \cdot m$ projector pixels into one uniformly colored one, ensuring that all *clusters* are illuminated. The optimal projections are then calculated only for this subset of combined pixel values. Now, each combined pixel illuminates all *clusters*, ensuring that the color-changing effect will always be correctly reproduced, regardless of the image content. However, because it combines multiple pixels into one, this approach significantly reduces the image resolution. To overcome this limitation, we realized another approach inspired by cluster-dot halftoning algorithms [1,

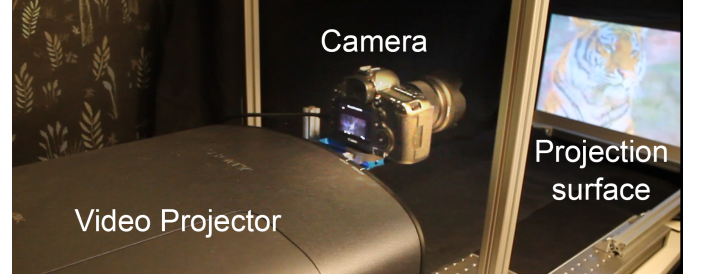


Fig. 5: Prototype for the color-changing application: A Canon 5DsR DSLR is used to register the Sony VPL-VW300ES projector to the patterned surface.

pp. 385-395], i.e., technique used in printing community. In this method, $P_{j,i}^{Opt}(x,y)$ is computed independently for each original projection pixel. The final image, however, is then assembled by applying *simplified dithering* [1, pp.385-491] to the optimized values. Dithering, in this context, relates to a method to apply spatial thresholding that preserves the overall image appearance. If pixel (x,y) is classified to the i -th *cluster*, only the optimal values from that cluster are assigned to it, and all other colorant values are discarded:

$$P_j^{Fin}(x,y) = \sum_{i=1}^K \delta_i(x,y) \cdot P_{j,i}^{Opt}(x,y) \quad (6)$$

$$\delta_i(x,y) = \begin{cases} 1; & (x,y) \in C_i \\ 0; & (x,y) \notin C_i \end{cases}$$

where $P_j^{Fin}(x,y)$ is the final intensity for the pixel position (x,y) and for the j -th color channel, and C_i is i -th cluster. The benefit of this *simplified dithering* approach is that it generates images in native projector resolution, preserving high-frequency details. This approach relies on the fact that the colorants are small and arranged in a high-frequency pattern, implying that, on average, it correctly creates the color-changing effect. In contrast to the previously mentioned pixel-combining approach, the *simplified dithering* does not guarantee that the color-changing effect will always be perfectly reproduced on each pixel, but it preserves the original image's resolution much better with its high-frequency content.

4) *Prototype*: To evaluate the proposed high-frequency pattern projection method for image alterations, we assembled a prototype (cf. Fig.5) using the following hardware components:

- **Printer**: An Epson Workforce WF-2750 inkjet printer



Fig. 6: Photographs of hue and chroma alterations. Left: Projection onto *pattern surface*. Right: The same projection onto the *white surface*. The upper row shows a slight hue shift of 45° . The center row more drastic hue shifts and in the bottom row a chroma change example is shown. (All images are taken with automatic aperture and white balance.)

(1440dpi) with standard inks was used to print the patterns.

- **Paper:** *Canon MP-101* paper was used.
- **Spectrophotometer:** A *Photoresearch PR 730* spectrophotometer was used to acquire spectral measurements with a resolution of $1nm$ for calibration.
- **Projector:** A *Sony VPL-VW300ES 4K LCoS* projector was used for the color-changing experiments. The response curves of this prosumer device required accurate calibration to ensure that $P_{j,i}^{Opt}$ resemble the device’s non-linearities (cf. Sec. IV-C1). Furthermore, in the projector settings, we were able to disable internal color processing.
- **Camera and lens:** A DSLR (Canon 5DsR, 8688x5792 pixels) with a high quality-prime lens with minimal chromatic aberrations (Sigma 50mm f/1.4 DG HSM Art) was used.

The proposed method can be realized with any other combination of similar components. The imaging characteristics of the optical elements as well as the device resolutions, however, have a strong impact on the overall quality.

5) *Color-Change Effects Using a Black and White Pattern:* In the following, we show results obtained by projecting onto a *b/w pattern surface* arranged as a 30° rotated checkerboard, using *spectral approach* and with three clusters deduced by the k-means algorithm.

a) *Hue and Chroma Alteration:* A potential application example is to alter the hue or chroma of the input image. Results are presented in Fig. 6²³. As shown in Fig. 4, the hue and chroma alterations preserve the lightness contrast of the projected image. However, when the hue-shift becomes larger, the image saturation decreases.

b) *Dual-Image Projections:* For a certain color range defined by the full color-changing sub-gamut, it is possible



Fig. 7: Photographs of dual-image projections. Left side: Projection onto the *pattern surface*. On the right, the same projection is shown on a *white surface*. One can observe that for a specific color range, we are able to alter between the images; however, lightness contrast is significantly reduced compared to hue and chroma alterations. (All images are taken with automatic aperture and white balance.)

to encode two completely different images. In Fig. 7³⁴, dual-images are shown in which two images are observed, one on the *pattern* and one on the *white surface*: While the content varies strongly, ghosting is minimal.

6) *Color-Change Effects Using a Color Pattern:* Our generic framework is not limited to *b/w* patterns, but can also create color-changing effects using a colored *pattern surface*, as described in Sec. III-B. Similar to Fig. 2b, the pattern contains *rgbcm* printed pigments, arranged in repetitive tiles rotated by 30° to avoid aliasing. K was set to 6. Fig. 8³ shows an example achieving a similar dual-image effect as with the *b/w* pattern.



Fig. 8: Photographs of dual-image projections: Projection onto the *pattern surface*. Right: The same projection onto *pattern surface*. It shows the same example as in Fig. 7, but created on a colored *pattern surface*. (All images are taken with automatic aperture and white balance.)

B. Monochrome-to-Color Conversion

Another sample application is the *monochrome-to-color projection* done by spatially illuminating high-frequency color patterns, similar to the electron-beam-based image formation in CRT screens. We realized this approach using a monochrome 365 nm UV projector illuminating fluorescent pigments emitting visible *rgb* light.

1) *Color-Prediction Accuracy and Achievable Color Gamuts:* Table II, shows the accuracy of the spectral

²(Standard License) shutterstock.com

³www.pexels.com (CC License)

⁴www.caminandes.com (CC), (c) copyright 2008, Blender Foundation www.bigbuckbunny.org



Fig. 9: UV-color projections. Gray: The calculated projection images. Colored: Photographs of the corresponding observed projection.

color-prediction model tested on a *pattern surface* containing *rgb* fluorescent pigments. They were arranged as repetitive tiles, similar to the ones in Fig. 2c. The number of k-means clusters was set to $K = 3$. Because in this case, the input only has three dimensions, we tested the color-prediction model on 125 spectral measurements covering the whole input projection space sub-sampled by the step width of 25% ($5^3 = 125$ measurements).

TABLE II: Prediction accuracy of the spectral prediction model predicting the the monochrome-to-color conversion

Monochrome to Color (ΔE_{00}^*)	mean	95% quantile	max
UV-Pattern surface	2.56	4.5	5.6

Because in this application, only one illumination channel j (i.e. projector color) exists, deducing the corresponding gamut becomes a simpler task. Furthermore, only one gamut needs to be computed, which describes all possible colors a monochromatic projection can achieve. To define the shape and volume of the color gamut, we again sub-sample the input projection space by a step width of 5% and predict the resulting CIELAB colors (Fig. 10). One can observe that the UV-projector gamut can achieve brighter colors compared to the projector gamut used for the color-changing application. However, the red fluorescent color is not as saturated as the greens and blues, creating a very narrow gamut volume leaving room for future investigations.

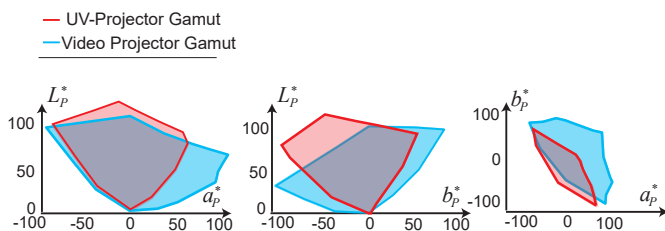


Fig. 10: Comparison between UV-projector gamut in red and video projector gamut in blue, as calculated from a *Sony VPL-VW300ES* 4K LCoS projector.

2) *Optimization Function*: Once we deduced the achievable color range of the UV-projection system, the optimal input intensities were calculated by minimizing the difference between the generated and target colors when projecting onto the fluorescent *patterns*:

$$P_i^{Opt} = \arg \min(\Delta E_{00}^*(Lab_{T_{rgP}}, Lab_P(P_i))) \quad (7)$$

where $Lab_{T_{rgP}}$ is the target CIELAB color that we want to observe on the fluorescent pattern surface, P_i^{Opt} is the optimal intensity that, when projected, produces a color as close as possible to the desired one, and $Lab_P(P_i)$ is a CIELAB

color observed on the pattern of the optimal projection. It is calculated by first predicting the reflectance using the color-prediction model and converting this value to CIELAB color space, as described in Sec.IV-C.

3) *Projection Image Generation*: The generation of the *monochrome-to-color* projections starts by specifying a single image that should be revealed when projecting onto the *pattern*. It is transformed to the projector image plane, and its colors are converted to CIELAB color space and gamut mapped to the estimated UV projector gamut. Then, for each pixel coordinate, the gamut mapped CIELAB color is used as the target color in Eq. 7, and the optimal input intensities are calculated. Finally, the single-channel projection image is assembled in an equivalent way as described in Sec. V-A3.

4) *Prototype*: The transformation of monochrome illumination to full-color images was evaluated on the UV projector prototype consisting of a custom manufactured DLP based 5 MP UV *In Vision Firebird* projector using a 365nm LED light source. The printed pattern was generated using transparent fluorescent ink which, when excited by the UV illumination, emits *rgb* wavelengths. It was printed on *BIO TOP 3 extra* paper, which is devoid of whitener that would lead to unwanted bluish fluorescent emissions. The other system components were the ones summarized in Sec.V-A4.

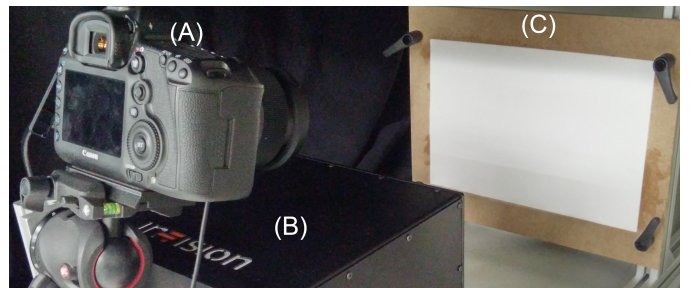


Fig. 11: Prototype for the monochrome-to-color application: The Canon 5DSR (A) is used to register the 365nm UV-projector (B) to the projection surface (C) containing transparent fluorescent red, green and blue inks.

5) *Results*: Fig. 9³ shows examples of the UV-to-color projection using *spectral approach* and with three clusters deduced by the k-means algorithm. One can observe that the green and blue colors are quite saturated, while the red component is slightly weaker, leaving room for further research. All the images are taken with aperture f/9, exposure 1/30s and ISO 300.

C. Implementation Details

All of the presented applications used the same generic processing pipeline. The geometric calibration-related algorithm steps were implemented in C++. For most parts, the

color-mapping operations were realized using Matlab. Because the image-based color optimization required a per-pixel constrained minimization for computing the optimal projection intensities (cf. Sec. IV-C2), the relatively slow Matlab interior point optimization was replaced by a multi-threaded C++ implementation using the *Bound Optimization BY Quadratic Approximation algorithm* [53], as implemented in the *dlib* library [54]. Computation times strongly depend on the chosen K and the number of projector channels (Computation times for 4K resolution on a standard workstation (Intel Xeon E5-1680 v3 3.2 GHz, 64 GB Ram, 1.0 TB Samsung 850 EVO SSD): ch=3, K=2: 13:35 minutes, ch=3, K=3: 41:44 minutes, ch=1, K=3: 2:26 minutes).

VI. EVALUATION AND DISCUSSION

As shown in Figs. 6 to 9, the proposed generic framework has a variety of applications. The achievable image quality is use-case dependent and influenced by several factors, such as: the pattern layout, dot size, and the number of clusters K used to classify the projected pixels. We discuss these factors in detail in the following.

A. Influence of Pattern Layout

The spatial pattern design strongly impacts the uniformity and clarity of the observed color. We present an evaluation on how to account for some undesirable effects that may occur depending on the layout, such as moiré artifacts or pattern visibility. For simplification, the evaluation was carried out using b/w patterns; however, the same principles can be applied to colored patterns, e.g. rgb or $cmymrgb$, as well. To investigate how the spatial layout influences the overall image quality, three different designs were compared:

- A b/w checkerboard
- A blue-noise random b/w distribution
- A 30° rotated b/w checkerboard

Each layout was registered, and clustered ($K = 2$). Fig.12a shows that when using a regular checkerboard, the interaction between the projected pixels and the printed colorants induces visual artifacts such as moiré and aliasing. Its strength depends on the pattern frequency with respect to the pixel size, e.g., the strongest moiré occurs if the checkerboard frequency is directly related to projector resolution. One solution to minimize moiré is to apply a blue-noise random distribution of the printed dots (Fig.12b). This random pattern was generated by halftoning a 50% gray intensity image with an blue-noise error-diffusion algorithm [55]. As can be seen, this efficiently suppresses moiré. However the benefit of using a regular pattern such as a checkerboard is that it is significantly less visually disturbing compared to a randomly distributed pattern of the same size, because the human eye is highly sensitive to detecting non-periodic spatial changes. For our applications, we used the rotated b/w checkerboard (Fig.12c), inspired by multi-color cluster-dot halftoning algorithms [1, pp. 429-458] [43, pp. 59-77]. The rotation of the printed with respect to the projection plane reduces the coupling of pixels, minimizing artifacts while at the same time having a low pattern visibility.

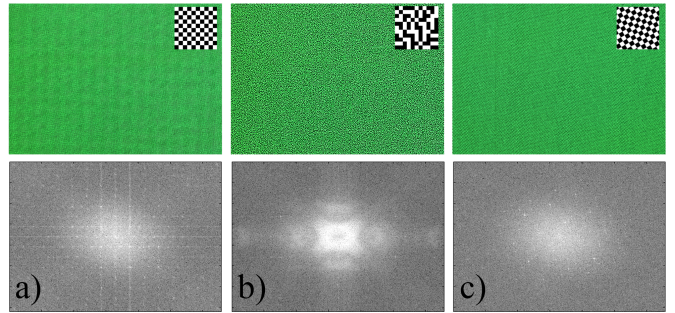


Fig. 12: Pattern comparison. Top row, one K -means cluster illuminated with a green projection, Bottom row, corresponding FFT spectra: (a) A standard high-frequency checkerboard generates strong aliasing artifacts which are also clearly visible in the spectral visualization In (b) the blue-noise random pattern shows no artifacts, but the structure is clearly visible. Rotating the checkerboard (c) minimizes the visibility as well as artifacts.

B. Size of Pattern Elements

The *pattern dot size* also affects the intensity of the generated colors. We evaluated different dot sizes: 1.0, 0.75, and 0.5mm on a surface size of 40x60cm, on a 30° rotated b/w checkerboard, by testing the intensity of the color-changing effect when switching surfaces.

We developed a method to evaluate both lightness and hue color changes for different dot sizes. It is divided into two stages. First, the intensity of the lightness-changing effect for achromatic colors is calculated, i.e., finding the range where we can freely change the lightness component of the color. Then, for this range, the intensity of hue-changing effect is estimated.

To deduce the lightness-changing ability, we use an approach adapted from Baar et. al. [33]. Fig. 13a1 left shows the formed area of all achievable lightness combinations. As shown in [33], fitting a rectangle inside this area defines a lightness range where the lightnesses between the *pattern* and *white surface* can be freely altered. Fig.13a2 left shows how different dot sizes influence the overall hue-changing effect. The bigger the dots the more pixels illuminate a single *colorant*, whereas for smaller dots more pixels will illuminate multiple *colorants*. However, bigger dots lead to a stronger pattern visibility and are thus more disturbing to observe. Furthermore, if the dots are enlarged too much, the eye will stop averaging the neighboring colors and the proposed color-generation effect will be lost.

This approach can be used to approximate the area for the desired color-changing effect. Furthermore, this approach is useful for large dimensional inputs of $P_{j,i}$, created with large K value, when using many *colorants*, when the sub-sampling approach of Pjanic and Hersch [31] is not feasible any more.

C. Number of Clusters

The chosen number for K directly impacts the range of achievable color alterations. As described in Sec.IV-B, the minimum value for K equals the number of colorants. Increasing K might give better control over the projection because it can exclusively illuminate specific *colorants* without using

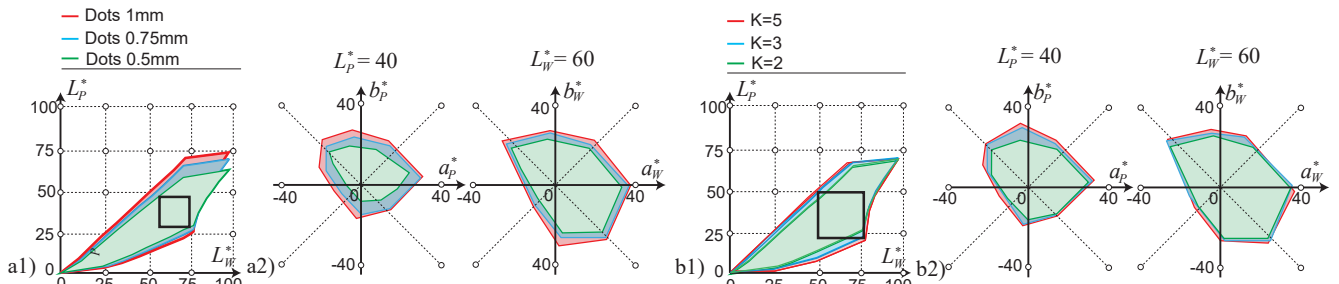


Fig. 13: Left: Achievable color-changing effect w.r.t. dot sizes. (a1) shows the lightness-changing ability for achromatic colors. The square defines the area where a free lightness change between the *pattern* and *white surface* is possible. (a2) represents the area where any color can change its hue by 180° . Right: Achievable color-changing effect w.r.t. different number of clusters (K). (b1) Shows the lightness changing ability for achromatic colors where the square represents the area where we can freely change the lightnesses between *pattern surface* and *white surface*. (b2) Represents the area where any color can change its hue by 180° .

the pixels that illuminate multiple *colorants*. In Fig.13, right, we show how different values for K affect the intensity of the color-changing effect. One can observe that as K increases, the achievable color change is increased as well. However, the speed of increasing the color-change decreases with higher K values. One can argue that $K = 3$ for b/w patterns is a good compromise because it increases the possible color change but does not increase the dimensionality input intensities $P_{j,i}$ significantly.

VII. LIMITATIONS AND FUTURE WORK

The proposed high-frequency pattern projection framework is based on modulating spatially neighboring projector pixels that then, in combination with the registered pattern, create a specific color-effect. This comes with the cost of a limited spatial resolution and, depending on the projector's resolution, the pattern structure is perceived when observing the projection surface from a short distance. As can be seen in the results and the video, for larger distances, the pattern structure is not disturbingly visible.

Besides the potential perception of the spatial pattern structure, the method also requires a gamut reduction of the projected content. The impact of this reduction heavily depends on the application use case. However, our proposed method to generate the maximum achievable sub-gamuts makes it straightforward to apply gamut-mapping operations while minimizing visual ghosting artifacts.

Furthermore, there is a physical limit regarding the intensity of the color-changing effect. The proposed color-changing framework relies on the property that the pattern surface darkens parts of the projection. This implies that lightnesses on the pattern surface are always lower than the lightness on a white surface. However, if one wants to achieve similar lightness ranges on both surfaces, a neutral gray surface can be used instead of a white one.

To achieve an acceptable image quality, an accurate registration is required. For both color-changing and UV-color projection prototypes, the proposed calibration method proved to be sufficiently accurate over several weeks. Because the projection surface is planar, one can imagine a quick single-image or on-line recalibration using an additional affine warping step of the projection image for situations in which the projector might have been slightly bumped.

Also, we acknowledge that there are other color spaces, that can represent the perceived color, such as CIECAM02 [20, pp. 287-301]. These color spaces account for various visual

effects, such as Stevens [20, pp. 127-129] and Hunt effect [20, pp. 125-127]. However, the goal of our paper is not to fully model the perceived color stimulus but to provide a general framework for generating the specific effects. In our proposed workflow, the color space can simply be changed if a more accurate color representation is needed.

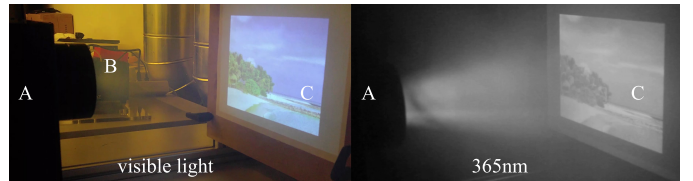


Fig. 14: The UV projector (A) enables the generation of color images (C) through participating media, in this case generated by a fog machine (B), without the perception of a frustum of scattered projector light since this is only generated outside of the visible spectrum (right).

VIII. SUMMARY AND CONCLUSIONS

We presented *Paxel*, an innovative projection framework relying on illuminating precisely registered high-frequency patterns as projection surfaces. The proposed general framework enables the application of several novel and interesting visual effects. These range from chroma and hue modifications to arbitrary dual-image projections, as well as single-channel to color projections. The latter enables the possibility of realizing a full-color projection system based on a single illumination wavelength in the UV spectrum, which, for example, enables invisible projection through participating media, such as fog, as shown in Fig.14. Furthermore, this approach allows one to triple the frame-rate of a gray-scale projector by trading spatial resolution for frame-rate. All these applications were actually realized as running prototypes and evaluated as such.

In the future, we are planning to further enhance the image quality by applying an automated adaptive out-of-gamut detection and a locally varying and temporally consistent compensation for such artifacts. Measuring and considering an accurate model of the projector's point spread function and more accurately compensating for its influence are two potential sources of improvement. Realizing an optimization capable of processing images in real-time for live-content is another direction of future research. Automatically deriving the optimized pattern layout for a specific setup based on parameters derived from a user evaluation is another interesting task for future investigation. Exploring different surfaces and inks that may have better absorption or UV-emission properties might significantly improve the color quality.

Potential applications of the proposed framework could be the usage of a visually eye-catching *color-changing effect* for art exhibitions, advertisements, or entertainment. Hidden content and messages with dual-projections are difficult to decode because one needs to know the used pattern, as well as the number of clusters. The decoding becomes increasingly difficult when using a high number of colorants and clusters which makes that method interesting for potential stenographic applications.

We believe that the core idea of our work, the combination of a precisely controlled, spatially varying illumination with high-frequency print patterns, has the potential to stimulate further research for an even wider range of applications.

APPENDIX A
TABLE OF TERMS

Table III shows the detailed description of all terminology used in this paper. The terminology covers fields of colorimetry, projection camera systems as well as optical-visual effects.

APPENDIX B

RESULTS ACHIEVED USING THE IMAGE-BASED APPROACH

In Fig. 15¹⁴, samples of a color-changing effect created with the image-based approach described in Sec. IV-C2 are presented. As can be seen, this approach can be used to generate color-changing effects as well. However, ghosting artifacts are more pronounced, because the color prediction is less accurate compared to the spectral approach.



Fig. 15: Photographs of Image-based approach: the left side shows projection onto the *b/w pattern surface*. On the right, the same projection is shown on a *white surface*. (All images are taken with automatic aperture and white balance.)

REFERENCES

[1] G. Sharma, *Digital Color Imaging Handbook*. Boca Raton, FL, USA: CRC Press, Inc., 2002.
 [2] M. D. Grossberg, H. Peri, S. K. Nayar, and P. N. Belhumeur, "Making one object look like another: controlling appearance using a projector-camera system," in *IEEE Computer Society Conference on Computer Vision and Pattern Recognition (CVPR)*, vol. 1, June 2004, pp. 452–459.
 [3] O. Bimber, A. Emmerling, and T. Klemmer, "Embedded Entertainment with Smart Projectors," vol. 38, no. 1. IEEE Computer Society Press, Jan 2005, pp. 48–55.
 [4] O. Bimber, G. Wetzstein, A. Emmerling, and C. Nitschke, "Enabling view-dependent stereoscopic projection in real environments," in *IEEE and ACM International Symposium on Mixed and Augmented Reality (ISMAR)*. IEEE, Oct 2005, pp. 14–23.
 [5] A. Grundhofer and O. Bimber, "Real-time adaptive radiometric compensation," in *IEEE Transactions on Visualization and Computer Graphics*, vol. 14, no. 1, Piscataway, NJ, USA, Jan. 2008, pp. 97–108.

TABLE III: Table of Terms

Term	Description
<i>Chroma and hue</i>	Appearance parameters of a color: <i>chroma</i> represents how much the color is saturated and <i>hue</i> refers to the according color family of a color, e.g., yellow, blue, red, magenta etc.
<i>CIELAB</i>	Perceptually uniform color-space deduced from CIEXYZ values [52, pp. 166-168].
<i>CIEXYZ</i>	Device independent color-space based on the color matching functions [52, pp. 156-157].
<i>Clusters</i>	Groups of projector pixels formed by the color similarity using a k-means algorithm.
<i>Colorants</i>	Individual colors that are present on the <i>pattern surface</i> .
<i>Color-changing effect</i>	Optical effect describing the modification of the color when the projection surface is changed.
<i>Color prediction model</i>	Model that enables us to predict the observed colors.
<i>Color reproduction workflow</i>	Workflow describing how to reproduce the desired color on the specific medium.
<i>DLP projector</i>	(Digital Light Processing) projector that uses one or multiple digital micromirror devices (DMD) to modulate light.
<i>Dual-image projections</i>	<i>Color-changing effect</i> that enables encoding two images within one projection. One image is revealed when projecting onto the <i>pattern surface</i> and another one when projecting onto the <i>white surface</i> .
<i>Nodal image</i>	Image of the scene as it would have been taken from a camera at the projectors perspective calculated using the <i>procams</i> calibration
<i>Pattern surface</i>	Projection surface containing the printed high frequency patterns.
<i>Procams</i>	Projector-camera system used to estimate the geometric relationship between the used projectors and cameras.
<i>Projector color</i>	An individual projected color channel.
<i>Reflectance</i>	Intensity of the light (per wavelength) reflected of the surface.
<i>Sub-gamut</i>	Collection of colors represented by a volume within a specific color space.
<i>Vignetting and defocus</i>	Projection artifacts commonly occurring at the edges of the projection surface: vignetting describes the amount of spatial brightness reduction and defocus the amount of blurring.
<i>White surface</i>	White-blank projection surface without any high frequency patterns.
ΔE_{00}^*	(Delta E CIE 2000) color-metric that quantifies the difference between two colors. [20, pp. 83]

[6] D. Wang, I. Sato, T. Okabe, and Y. Sato, "Radiometric compensation in a projector-camera system based properties of human vision system," in *IEEE Computer Society Conference on Computer Vision and Pattern Recognition - Workshops (CVPRW)*. Washington, DC, USA: IEEE Computer Society, Jun 2005.
 [7] M. Ashdown, T. Okabe, I. Sato, and Y. Sato, "Robust content-dependent photometric projector compensation," in *IEEE Computer Society Conference on Computer Vision and Pattern Recognition - Workshops (CVPRW)*. Washington, DC, USA: IEEE Computer Society, Jun 2006.
 [8] A. Grundhofer and D. Iwai, "Robust, error-tolerant photometric projector compensation," in *IEEE Transactions on Image Processing*, vol. 24, no. 12, 2015, pp. 5086–5099.

- [9] G. Wetzstein and O. Bimber, "Radiometric Compensation of Global Illumination Effects With Projector-Camera Systems," in *ACM SIGGRAPH Research Posters*. ACM Press, Jul 2006, p. 38.
- [10] D. G. Aliaga, Y. H. Yeung, A. Law, B. Sajadi, and A. Majumder, "Fast high-resolution appearance editing using superimposed projections," in *ACM Transactions on Graphics*, vol. 31, no. 2. New York, NY, USA: ACM, April 2012, pp. 13:1–13:13.
- [11] A. Bermanno, P. Brüscheiler, A. Grundhöfer, D. Iwai, B. Bickel, and M. H. Gross, "Augmenting physical avatars using projector-based illumination," in *ACM Transactions on Graphics (Proc. SIGGRAPH Asia)*, vol. 32, no. 6. New York, NY, USA: ACM, Nov. 2013, pp. 189:1–189:10.
- [12] H. Park, M.-H. Lee, B.-K. Seo, H.-C. Shin, and J.-I. Park, "Radiometrically-compensated projection onto non-lambertian surface using multiple overlapping projectors," in *Proceedings of the First Pacific Rim Conference on Advances in Image and Video Technology*, ser. PSIVT'06. Berlin, Heidelberg: Springer-Verlag, 2006, pp. 534–544.
- [13] K. Fujii, M. D. Grossberg, and S. K. Nayar, "A projector-camera system with real-time photometric adaptation for dynamic environments," in *IEEE Computer Society Conference on Computer Vision and Pattern Recognition (CVPR)*, vol. 1, June 2005, pp. 814–821.
- [14] O. Bimber and D. Iwai, "Superimposing dynamic range," in *ACM Transactions on Graphics (Proc. SIGGRAPH Asia)*, vol. 27, no. 5. New York, NY, USA: ACM, 2008, pp. 150:1–150:8.
- [15] S. Shimazu, D. Iwai, and K. Sato, "3d high dynamic range display system," in *IEEE and ACM International Symposium on Mixed and Augmented Reality (ISMAR)*. IEEE, 2011, pp. 235–236.
- [16] B. R. Jones, R. Sodhi, P. Budhiraja, K. Karsch, B. Bailey, and D. Forsyth, "Projectibles: Optimizing surface color for projection," in *Proc. 28th Annual ACM Symposium on User Interface Software and Technology (UIST)*. New York, NY, USA: ACM, 2015, pp. 137–146.
- [17] T. Amano, "Coded facial expression," in *ACM SIGGRAPH Asia Emerging Technologies*. New York, NY, USA: ACM, 2016, pp. 11:1–11:2.
- [18] T. Kawabe, M. Sawayama, and S. Nishida, "Deformation lamps: A projection technique to make a static picture dynamic," in *ACM SIGGRAPH Emerging Technologies*. New York, NY, USA: ACM, 2015, pp. 8:1–8:1.
- [19] T. Sun, G. Pettitt, N. T. Ho, K. Eckles, B. Clifton, and B. Cheng, "Full color, high contrast front projection on black emissive display," in *SPIE Emerging Digital Micromirror Device Based Systems and Applications IV*, vol. 8254, Mar. 2012.
- [20] M. D. Fairchild, *Color Appearance Models*, ser. The Wiley series on imaging science and technology. New York: Wiley, 2013, a Wiley-Interscience publication.
- [21] H. Wallach, "Brightness constancy and the nature of achromatic colors," in *Journal of Experimental Psychology*, vol. 38, no. 3, 1948, pp. 310–324.
- [22] E. H. Land and J. J. McCann, "Lightness and retinex theory," in *Journal of the Optical Society of America*, vol. 61, no. 1. OSA, 1971, pp. 1–11.
- [23] M. E. Rudd and I. K. Zemach, "Quantitative properties of achromatic color induction: an edge integration analysis," in *Vision Research*, vol. 44, no. 10, 2004, pp. 971–981.
- [24] G. Gronchi and E. Provenzi, "A variational model for context-driven effects in perception and cognition," in *Journal of Mathematical Psychology*, vol. 77, no. 3, 2017, pp. 124–141.
- [25] P. Vangorp, K. Myszkowski, E. W. Graf, and R. K. Mantiuk, "A model of local adaptation," in *ACM Transactions on Graphics (Proc. SIGGRAPH Asia)*, no. 6. ACM, 2015, pp. 166:1–166:13.
- [26] A. Bermanno, I. Baran, M. Alexa, and W. Matusk, "Shadowpix: Multiple images from self shadowing," in *Comput. Graph. Forum*, vol. 31, no. 2.3. Chichester, UK: The Eurographics Association & John Wiley & Sons, Ltd., 2012, pp. 593–602.
- [27] M. Papas, T. Houit, D. Nowrouzezahrai, M. Gross, and W. Jarosz, "The magic lens: Refractive steganography," in *ACM Transactions on Graphics (Proc. SIGGRAPH Asia)*, vol. 31, no. 6. New York, NY, USA: ACM, Nov. 2012, pp. 186:1–186:10.
- [28] R. D. Hersch, F. Collaud, and P. Emmel, "Reproducing color images with embedded metallic patterns," in *ACM Transactions on Graphics (Proc. SIGGRAPH)*, vol. 22, no. 3. New York, NY, USA: ACM, Jul. 2003, pp. 427–434.
- [29] R. D. Hersch, P. Donzé, and S. Chosson, "Color images visible under uv light," in *ACM Transactions on Graphics (Proc. SIGGRAPH)*, vol. 26, no. 3. New York, NY, USA: ACM, Jul. 2007, pp. 75:1–75:9.
- [30] R. D. Hersch and S. Chosson, "Band moiré images," in *ACM Transactions on Graphics (Proc. SIGGRAPH)*, vol. 23, no. 3. New York, NY, USA: ACM, Aug. 2004, pp. 239–247.
- [31] P. Pjanic and R. D. Hersch, "Color changing effects with anisotropic halftone prints on metal," in *ACM Transactions on Graphics (Proc. SIGGRAPH)*, vol. 34, no. 6. New York, NY, USA: ACM, Oct. 2015, pp. 167:1–167:12.
- [32] —, "Color imaging and pattern hiding on a metallic substrate," in *ACM Transactions on Graphics (Proc. SIGGRAPH)*, vol. 34, no. 4. New York, NY, USA: ACM, Jul. 2015, pp. 130:1–130:10.
- [33] T. Baar, M. Shahpaski, and M. V. O. Segovia, "Image ghosting reduction in lenticular relief prints," in *Proc. SPIE, Measuring, Modeling, and Reproducing Material Appearance*, vol. 9018. SPIE-IS&T, 2014, pp. 90180N:1–90180N:7.
- [34] H. Young-Chang, "Visual cryptography for color images," in *Pattern Recognition*, vol. 36, no. 7, 2003, pp. 1619 – 1629.
- [35] M. Naor and A. Shamir, *Visual Cryptography*, A. De Santis, Ed. Berlin, Heidelberg: Springer Berlin Heidelberg, 1995.
- [36] S. Abdulla, "New visual cryptography algorithm for colored image," in *Journal of Computing, Cryptography and Security*, vol. 2, no. 4, 2010, pp. 21 – 25.
- [37] S. M. Chosson and R. D. Hersch, "Beating shapes relying on moiré level lines," in *ACM Transactions on Graphics (Proc. SIGGRAPH)*, vol. 34, no. 1. New York, NY, USA: ACM, Dec. 2014, pp. 9:1–9:11.
- [38] T. L. Turner and R. F. Hellbaum, "Lc shutter glasses provide 3-d display for simulated flight," in *Information Display*, vol. 2, no. 9. Santa Ana, CA, USA: Society for Information Display, Sep. 1986, pp. 22–24.
- [39] H. Jorke, A. Simon, and M. Fritz, "Advanced stereo projection using interference filters," in *3DTV Conference: The True Vision - Capture, Transmission and Display of 3D Video*, May 2008, pp. 177–180.
- [40] R. Zone, *3-D Revolution: The History of Modern Stereoscopic Cinema*. University Press of Kentucky, 2012.
- [41] M. Hirsch, G. Wetzstein, and R. Raskar, "A compressive light field projection system," in *ACM Transactions on Graphics (Proc. SIGGRAPH)*, vol. 33, no. 4. New York, NY, USA: ACM, Jul. 2014, pp. 58:1–58:12.
- [42] B. Masia, G. Wetzstein, P. Didyk, and D. Gutierrez, "A survey on computational displays: Pushing the boundaries of optics, computation, and perception," in *Computers & Graphics*, vol. 37, no. 8. Pergamon, 2013, pp. 1012–1038.
- [43] I. Amidror, *The Theory of the Moiré Phenomenon: Volume 1 (Computational Imaging and Vision)*. Springer, 2009.
- [44] O. Choi, H. Lim, and S. C. Ahn, "Robust binarization of gray-coded pattern images for smart projectors," in *International Conference on Electronics, Information, and Communications (ICEIC)*, Jan 2016, pp. 1–4.
- [45] J. Salvi, S. Fernandez, T. Pribanic, and X. Llado, "A state of the art in structured light patterns for surface profilometry," in *Pattern Recognition*, vol. 43, no. 8. New York, NY, USA: Elsevier Science Inc., Aug. 2010, pp. 2666–2680.
- [46] B. Delaunay, "Sur la sphère vide. A la mémoire de Georges Voronoï," in *Bulletin de l'Académie des Sciences de l'URSS*, no. 6, 1934, pp. 793–800.
- [47] H. Chang, O. Fried, Y. Liu, S. DiVerdi, and A. Finkelstein, "Palette-based photo recoloring," in *ACM Transactions on Graphics (Proc. SIGGRAPH)*, vol. 34, no. 4. New York, NY, USA: ACM, 2015, pp. 139:1–139:11.
- [48] S. Lloyd, "Least squares quantization in pcm," in *IEEE Transactions on Information Theory*, vol. 28, no. 2. Piscataway, NJ, USA: IEEE Press, Sep. 1982, pp. 129–137.
- [49] S. Zhang, *High-Speed 3D Imaging with Digital Fringe Projection Techniques*. Boca Raton, FL, USA: CRC Press, Inc., 2016.
- [50] P. S. Huang., C. Zhang, and F. Chiang, "High-speed 3-d shape measurement based on digital fringe projection," in *Optical Engineering*, vol. 42, no. 1, 2003, pp. 163–168.
- [51] J. Duchon, "Splines minimizing rotation-invariant semi-norms in sobolev spaces," in *Constructive Theory of Functions of Several Variables: Proceedings of a Conference Held at Oberwolfach April 25 – May 1, 1976*, W. Schempp and K. Zeller, Eds. Berlin, Heidelberg: Springer Berlin Heidelberg, 1977, pp. 85–100.
- [52] G. Wyszecki and W. S. Stiles, *Color science : concepts and methods, quantitative data and formulae*, ser. The Wiley series in pure and applied optics. New York: Wiley, 1982, a Wiley-Interscience publication.
- [53] M. J. D. Powell, *The BOBYQA algorithm for bound constrained optimization without derivatives*. Technical Report, Department of Applied Mathematics and Theoretical Physics, Cambridge University.
- [54] D. E. King, "Dlib-ml: A machine learning toolkit," in *Journal of Machine Learning Research*, vol. 10, 2009, pp. 1755–1758.
- [55] B. Zhou and X. Fang, "Improving mid-tone quality of variable-coefficient error diffusion using threshold modulation," in *ACM Transactions on Graphics (Proc. SIGGRAPH)*, vol. 22, no. 3. New York, NY, USA: ACM, Jul. 2003, pp. 437–444.